SYNTHETIC APERTURE SONAR IMAGING USING AN UNMANNED UNDERWATER VEHICLE

TJ Sutton[1], HD Griffiths[1] and J Robinson[2]

(1) Dept of Electronic and Electrical Engineering, University College London, Torrington Place, London WC1E 7JE
(2) Thales Underwater Systems, Ocean House, Templecombe, Somerset BA8 0DH

1. INTRODUCTION

Synthetic aperture sonar is the application in an undersea environment of the technology of synthetic aperture radar (SAR), a technique for high-resolution imaging using a small moving antenna [1-3]. In synthetic aperture systems, a sequence of radar (or sonar) returns are recorded as the moving platform travels in a nominally straight line past the target area of interest. The returns are combined coherently as though they had been received by a single, long antenna. Operating underwater to image the seabed, synthetic aperture sonar (SAS) systems are of military interest for minehunting, while civilian uses might include the identification of pipelines, cables, waste canisters, wrecks and so on.

The central problem holding back the development of synthetic aperture sonar systems for high-resolution imaging of the seabed has been the need to measure and compensate accurately for across-track errors (sway and yaw) in the motion of the sonar platform. In the case of a high-frequency imaging system for mine hunting, departures of just a few millimetres from the nominal straight track will seriously degrade the image obtained. The problem is particularly acute for SAS systems because the underwater platform moves relatively slowly and some tens of seconds may be needed to form the synthetic aperture. The across-track motion of the sonar platform involves very small accelerations that are difficult to measure accurately in the presence of vehicle vibration. Instead, research has been directed toward using the sonar returns themselves to estimate and correct for the platform motion, a process termed *autofocus.*

Earlier studies using rail-based systems have laid the groundwork for a series of trials led by QinetiQ that took place in March 2001 using a full-scale self-propelled unmanned underwater vehicle, 7 m in length. An array of 192 hydrophones were used to sample the sound field due to a set of targets placed at a range of several hundred metres in a shallow water coastal environment. UCL have analysed the data as part of an EPSRC/Thales Underwater Systems/QinetiQ project to investigate motion compensation techniques for high-resolution spotlight and squint mode synthetic aperture sonar. The paper shows how actual vehicle motions can be compensated fully for motion errors using the displaced phase centres (DPC) and phase gradient autofocus (PGA) algorithms. Images have been generated of target objects at ranges in excess of 250 m at resolutions of a few tens of millimetres.

2. AUTOFOCUS

Autofocus is relatively straightforward if the scene contains a prominent point scatterer. As the vehicle passes, the scatterer gives rise to a predictable, hyperbolic trace (after range compression) whose

exact characteristic depends on range. Departures from the expected curve indicate across-track platform motion or medium inhomogeneity [4]. The pioneering early SAS trials using towed underwater vehicles such as the Kiwi-SAS (1994 trials) and the SAMI (1995/6 trials) used prominent point processing (PPP) autofocus [5-7]. However, in general the seabed does not contain strong point scatterers, while mines are naturally designed to have low scattering strength to avoid detection.

A widely used and highly effective method of autofocus is the displaced phase centres (DPC) method, in which overlapping phase centres are cross-correlated between one ping to the next, giving two measurements at different times from nominally the same point in space. The method uses the texture of the seabed as a whole and does not rely on the existence of highly reflective point scatterers. DPC has been applied to SAS by Sheriff [8] and developed to identify platform surge, sway and yaw by Pinto, Billon and others [9-12]. However, the accuracy with which yaw angle can be identified falls away if the platform speed is increased, because only a few phase centres overlap; in this case, estimates of the change in platform angle between pings is highly susceptible to noise [10].

An alternative method of yaw removal is the phase gradient algorithm (PGA), a well-established method of removing phase error from SAR images [13-15]. PGA has the advantage of being essentially a feedback technique, in that it generates whatever phase error is needed to focus the image, while DPC is an open-loop approach, measuring the vehicle motion by cross-correlation and using this measurement to correct the image. DPC requires careful calibration of the hydrophones and data acquisition equipment in order to achieve the Cremer-Rao lower bound [10].

3. 'PATHFINDER' UUV TRIALS, PORTLAND HARBOUR, MARCH 2001

3.1 SUMMARY OF TRIALS

Under the former DERA Priority Pathfinder scheme for jointly-funded research, a three-year project was set up to investigate how to integrate a high quality wideband minehunting sonar onto a 21" diameter UUV. The project partners were QinetiQ (formerly DERA), Thales Underwater Systems (formerly Thomson Marconi Sonar) and BAE Systems [17]. The vehicle was some 7 m in length and propelled electrically at 1-2 m/s using internal batteries (Figure 1), and was able to carry both forward-looking and side-looking sonar systems. Communication with the vehicle was possible using a low-bandwidth acoustic link for essential monitoring and emergency retrieval; but the main communication and data transfer was through a high-bandwidth (2.5 Gbit/s) optical fibre link.

Figure 2 shows the installed side-looking transmitter and hydrophone array. The sonar equipment was designed, built and integrated into the UUV by Thales Underwater Systems and QinetiQ. The receiver comprised six 32-element linear hydrophone arrays placed in a line to give a linear array of 192 hydrophones. The separation of the hydrophones was 5.8 mm. At the carrier frequency, the physical beamwidth available with the array was less than one degree. The sonar data were demodulated digitally and then sampled at 75 kHz for subsequent analysis.

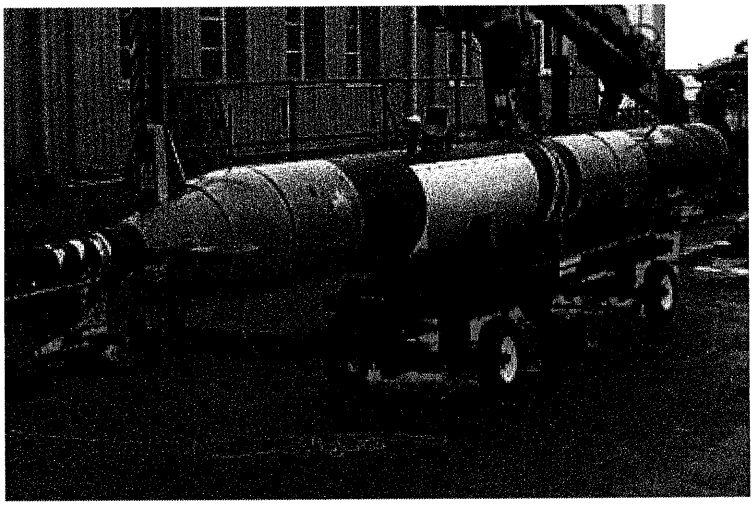

Figure 1 *The Pathfinder UUV mine reconnaissance demonstrator*

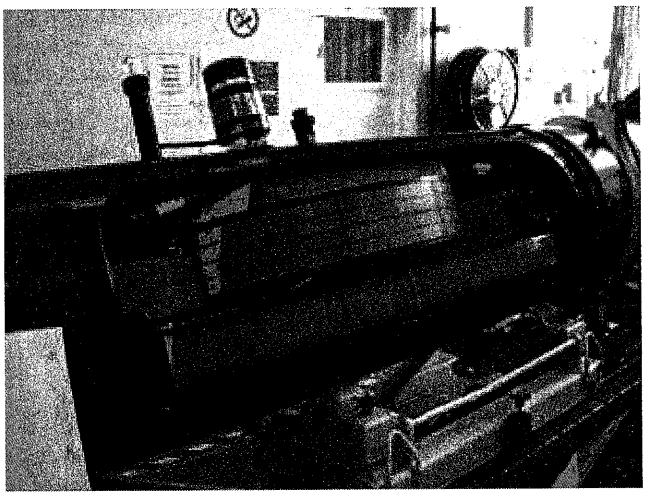

Figure 2 *Configuration of side-looking sonar transmitter (curved) and hydrophone array*

3.2 IMAGING USING THE PATHFINDER TRIALS DATA

Figure 3 shows the calculation scheme for synthetic aperture imaging. There are three stages of motion compensation:

(1) Direct compensation using the Inertial Navigation System (INS), in which the measured motions are projected into the slant range plane and used to apply a time advance or delay to the measured sonar returns received at each phase centre.
(2) Phase centres that are nominally coincident from one ping to the next are cross-correlated to determine platform sway (in the slant range plane) and again the results are applied to the data as an advance or delay to the sonar returns.

(3) Phase errors across the final image are extracted iteratively by means of the phase gradient autofocus algorithm.

If motion compensation is applied to the sonar data using the INS alone, including all six degrees of freedom, a spotlight image of a target at 100 m made using a track length of 25 m takes the form shown in Figure 4. The vehicle was travelling at 1 m/s. The image is poorly focused in azimuth and little structure can be seen.

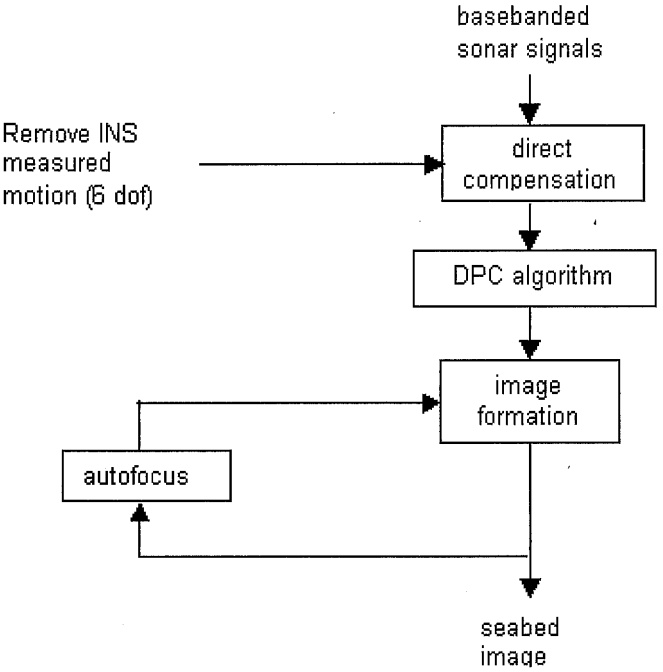

Figure 3 *Analysis scheme for synthetic aperture sonar*

With INS compensation the object is fairly clearly defined in range, although the phase errors are too large for successful focusing in azimuth. The main contribution of the INS is to identify the across-track drift of the platform. In this run the platform drifts across track by 1 m in a track length of 25 m due to tidal action. A Doppler velocity log was used to identify across-track velocity. When this motion error is corrected, the features of the target are represented in the image at roughly at the correct range, although they remain defocused in azimuth.

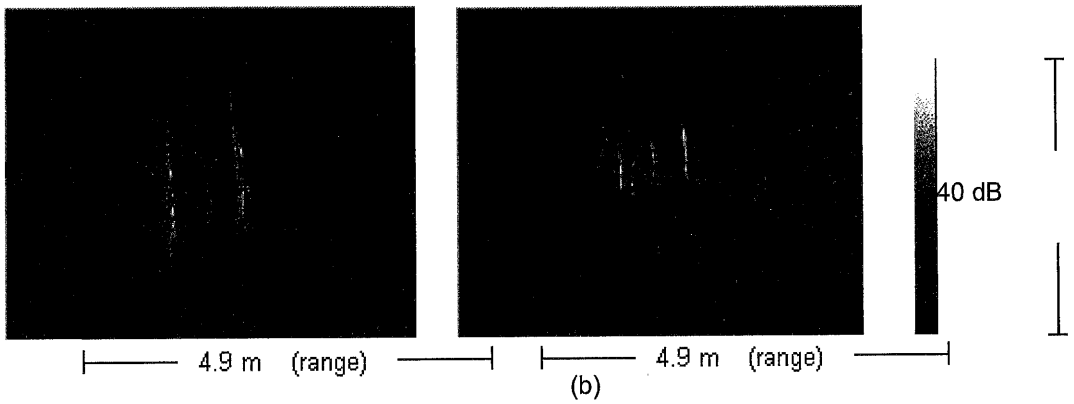

Figure 4 *Spotlight image of target at 105 m, Pathfinder run 7. (a) Motion compensation using INS alone, six degrees of freedom.(b)Motion compensation using DPC alone (no yaw measurement)*

When the DPC algorithm is used with no INS contribution, Figure 4(b) results. Here the DPC algorithm is used only to measure sway motion; there is no yaw measurement. The image is now placed correctly in range. However, the azimuth focus remains poor due to remaining small errors. The DPC algorithm detects small, relatively high-frequency motions of the vehicle that are very important for motion compensation.

In Figure 5 the measured yaw was applied to correct the data and followed by DPC autofocus. The other INS measurements were omitted. The azimuth focus is further improved, as might be expected since there is otherwise no compensation for yaw.

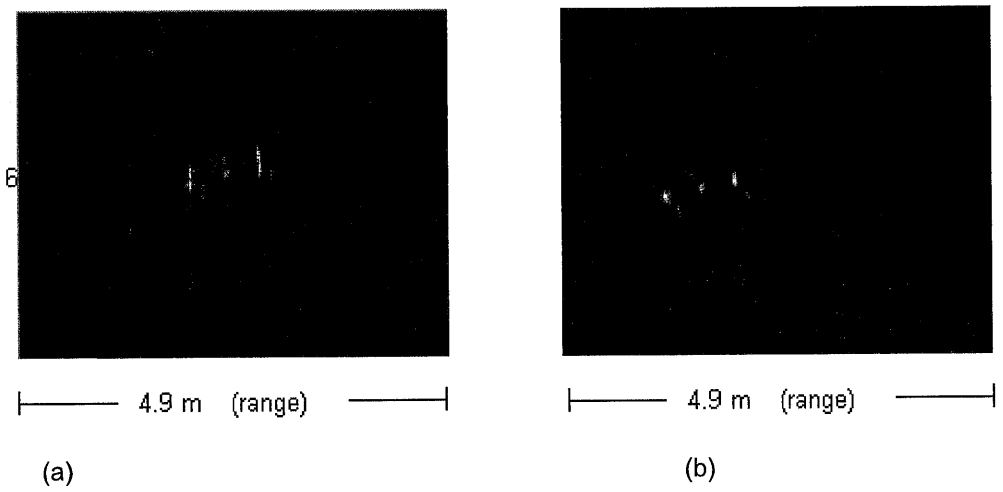

Figure 5 *Spotlight image of target at 105 m, Pathfinder run 7. (a) Motion compensation using INS measured yaw (only) followed by sway estimate using the DPC algorithm (b) Motion compensation using INS yaw measurement, DPC sway correction and PGA.*

The measured yaw is shown in Figure 8(b) (dashed trace). The total variation during the run was less than one degree.

After direct compensation and use of the DPC algorithm, the phase gradient algorithm may be used to remove remaining phase errors. Three iterations of the algorithm applied to the image with yaw

and DPC correction, Figure 5(a), resulted in the focused image Figure 5(b). In Figure 5(b) the target structure has come into focus as well as the pointlike scatterers. The target peaks are 40 dB above the surrounding background, which is thought to be limited by multipath scattering from the moving sea surface. The artefacts toward the bottom of the image are due to grating lobes (sampled once/ping). The nature of the phase characteristic that is extracted by the PGA algorithm is discussed below.

Figure 6 shows targets at 40 m and 207 m. At long ranges the background noise is increased due to multipath reflections from the moving sea surface.

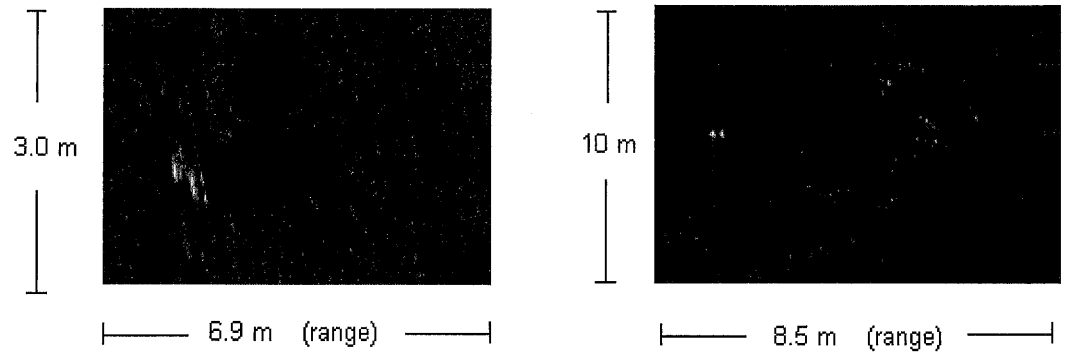

Figure 6 (a) *Squint-mode image of target at 40 m. Squint angle 15 deg. Motion compensation: DPC (surge and sway). Note shadow thrown by the target object. (b) Spotlight image of target at 207 m. The track length was 20 m. Motion compensation: DPC (surge, sway) with PGA autofocus. The peak is 38 dB above the noise floor.*

4. APPLICATION OF PGA ALGORITHM TO SYNTHETIC APERTURE SONAR

4.1 PGA AND RANGE CURVATURE

The phase gradient algorithm (PGA) was published by Eichel of Sandia National Laboratories, New Mexico in 1989 [13-15]. It is a method of extracting the phase error from a spotlight-mode SAR image, that is, one in which the antenna is steered to maintain a chosen target area in view. Correction of the phase error focuses the image.

Neglecting range migration effects for the moment, the Doppler phase of the *n*th range line after range compression is a function of along-track distance *u* and takes the form of a sum of contributions due to *m* scatterers:

$$g_n(u) = \sum_m A_{mn} \exp\left(-jK_n(x_m - u)^2\right)\exp\left(j\phi_e(u)\right) \qquad (1)$$

Here $\phi_e(u)$ is the phase error due to platform motion and medium inhomogeneity, K_n is a range-dependent focus parameter and x_m is the along-track location of the *m*th point scatterer. In spotlight-mode processing for SAR, each range line is conventionally multiplied by conjugate of the point spread response for a scatterer at u=0 and the Fourier transform is taken (deramp processing) [10]. After multiplication the *n*th range line then takes the form (dropping constant value multipliers):

$$f_n(u) = \sum_m \exp(jk_m u)\exp(j\phi_e(u)) \tag{2}$$

in which k_m is a wavenumber which is proportional to scatterer location x_m. The Fourier transform of $f_n(u)$, taken over a track of length S_L, is then:

$$F_n(k_u) = \sum_m \mathrm{sinc}\left[\frac{S_L}{2\pi}(k_m - k_u)\right] \otimes \Phi(k_u) \tag{4}$$

where $\otimes$ denotes convolution, k_U is wavenumber in the u direction and $\Phi(k_U)$ is a blurring function equal to the Fourier transform of $\exp(j\phi_e(u))$. $F_n(k_U)$ is a set of blurred point scatterers spread out along the k_U axis according to the values of k_m. In order to extract the phase gradient from Eq (3), the strongest scatterer is chosen and the whole range line is shifted circularly to place the strongest scatterer at the origin, $k_U = 0$. A window is then applied to preserve the width of the dominant 'blur' while excluding the contributions of the other scatterers as far as possible. The inverse Fourier transform then yields an estimate of $\exp(j\phi_e)$. Combining many range lines, a minimum-variance estimate of the gradient of phase can be extracted [15]; the phase itself then follows by integration.

Some care is required when implementing the PGA algorithm for SAS. The main issue is range migration. The range increments used in SAS are much narrower than those of SAR; typical SAS range lines are a single carrier wavelength in width rather than perhaps 30 wavelengths for an aircraft-borne SAR. In SAS the conventional sidescan response of a point scatterer after range compression will generally migrate through many range bins over the track length of interest, due to range curvature as indicated in Figure 7(a). An Equation of the form (1) is only arrived at after removing the effect of range migration, for example by interpolation in the Doppler (azimuth wavenumber) domain as in the range-Doppler algorithm. The process of range migration correction is indicated schematically in Figures 7(b) and (c). The existence of a phase error, $\phi_e(u)$, gives rise to two difficulties:

(1) Across-track range errors of more than a carrier wavelength will cause the response of a single scatterer to be divided among more than one range line, despite the correction of range migration. The phase error estimate derived from each individual range line will therefore be based on only a fragment of the expected aperture.
(2) More seriously, the phase error introduces additional spatial frequencies in azimuth which are not placed in the correct range bins when the range migration correction is carried out. The response of Eq (1) is therefore spread among a number of adjacent range lines.

Both these problems can be alleviated if groups of adjacent range lines are summed together before the PGA algorithm is applied. The number of lines depends on the frequency content of the across-track range error.

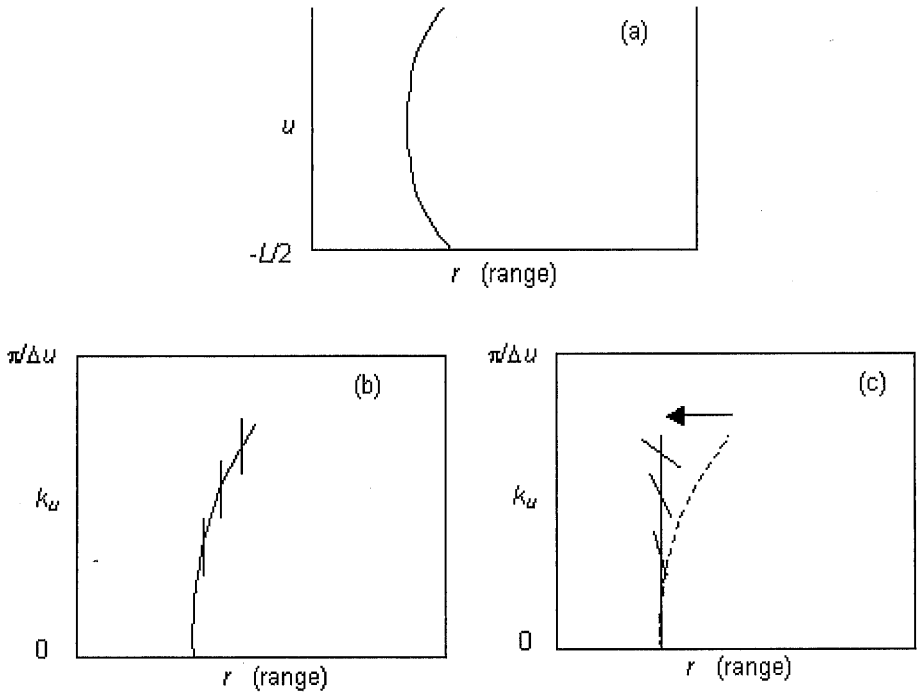

Figure 7 *(a) Sketch of the response of a point scatterer in the range-azimuth domain (spotlight mode). Motion errors are too small to be seen. (b) Sketch of the response of a point scatterer in the range-Doppler (wavenumber) domain. The error-free response (curve) is convolved with the transform of the motion error (vertical bars) to give a blurred area; (c) the effect of range migration correction in the range-Doppler domain.*

4.2 APPLICATION TO PATHFINDER DATA

In Figure 5 above it was seen that PGA was effective in focusing an image by removing the residual phase error after direct yaw compensation and DPC motion correction. Although not shown, a similar well-focused image results if the PGA algorithm is applied to the data corrected using DPC but with *no* direct yaw compensation (*i.e.* to improve Figure 4(b)). It is of interest to compare the phase errors that result in the two cases.

Figure 8(a) shows the phase errors with and without direct yaw compensation. The solid line is the phase error (expressed as across-track range error in mm) with yaw corrected directly, while the dashed line is with no yaw correction. Since the final image was well-focused in both cases, the difference arises from the additional platform yaw which was removed by PGA in the second (dashed) case.

After the platform sway has been corrected, the remaining yaw is related to the range error by the geometry of the situation:

$$yaw = \frac{dr_{err}}{du} \qquad (4)$$

in which r_{err} is the across-track range error towards the scene, u is distance along track in the azimuth direction and the yaw is expressed in radians (small angles assumed).

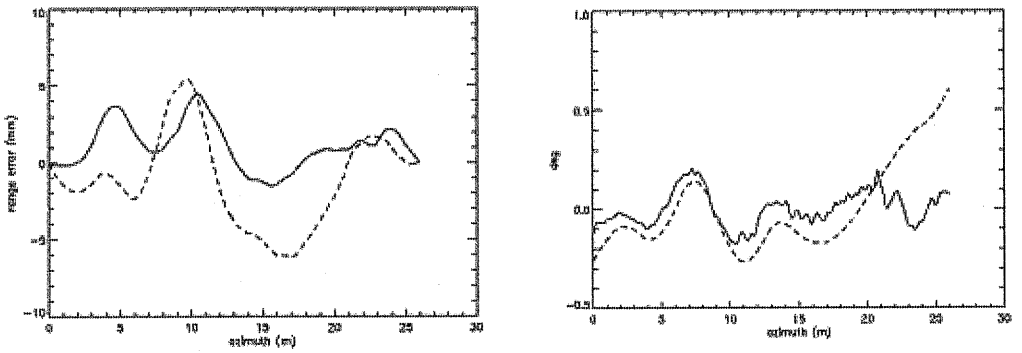

Figure 8 (a) *Comparison of the range error identified by PGA for target at 105 m. Solid line, with direct yaw compensation (see Figure 5(a)); dashed line, without direct yaw compensation. (b) Solid line: The rate of change of the difference between the two curves of (a). The dashed line is the measured yaw (INS).*

Figure 8(b) shows the rate of change of the difference in range error with and without yaw (solid line) against the measured yaw. There is clear agreement over the early part of the azimuth travel distance, showing that the PGA has correctly identified the main features of the platform yaw motion. Note that since the range error is the integral of yaw the range errors have low spatial frequency content and so are relatively easy to correct. The difference between traces arises because PGA also removes the effect of other errors and approximations introduced during the imaging process.

5. CONCLUSIONS

A frequency-domain synthetic aperture sonar imaging system has been implemented in which there are three levels of motion compensation: direct compensation using sway, yaw and other variables measured by the on-board Inertial Navigation System; correlation-based autofocus using the

Displaced Phase Centres (DPC) algorithm; and removal of phase errors using the Phase Gradient Autofocus (PGA) algorithm. The system has been used to calculate images using data collected by the TUS/QinetiQ/BAE Systems 'Pathfinder' UUV trials.

The DPC algorithm has been implemented without yaw estimation to avoid loss of accuracy at high platform speeds (low overlap of phase centres). It is demonstrated that the PGA effectively compensates for yaw errors that remain in the image after DPC compensation. The range error detected by PGA is the integral of the yaw error as expected, so tends to contain only low-wavenumber components. However, if the measured yaw error is used to compensate the data directly, the resulting image after DPC is better, while the range error detected by PGA is reduced.

Images from the Pathfinder trials have been generated for targets at up to 260 m with resolutions of a few tens of millimetres. At longer ranges the low water depth (12 m) caused some additional background noise level due to multipath reflections from the moving sea surface.

6. ACKNOWLEDGEMENTS

The authors are pleased to acknowledge the support of EPSRC, Thales Underwater Systems, QinetiQ, and, in particular, Chris Emblen and Sean Chapman of QinetiQ for their major contributions.

7. REFERENCES

1. WILEY, C A 'Synthetic aperture radars – a paradigm for technology evolution', *IEEE Trans. Aerospace and Electronic Systems* **AES-21**, 1985, 440-443.
2. CUTRONA, L J, VIVIAN, W E, LEITH, E N and HALL, G O 'A high resolution radar combat surveillance system', *IRE Trans. Mil. Electron.* **5**, April 1961, 127-130.
3. CURLANDER, J C and McDONOUGH, R N 'Synthetic Aperture Radar – Systems and Signal Processing'. John Wiley & Sons, Inc, New York.
4. CARRARA, W G, GOODMAN, R S and MAJEWSKI, R M 'Spotlight Synthetic Aperture Radar – Signal Processing Algorithms' Artech House, Boston.
5. HAWKINS, D W and GOUGH, P T 'Recent sea trials of a synthetic aperture sonar' *Proc of the Institute of Acoustics* **17**(8), 1995, 1-10.
6. HAWKINS, D W 'Synthetic aperture imaging algorithms: with application to wide bandwidth sonar' PhD thesis, University of Canterbury, New Zealand, 1996.
7. CHATILLON, J, ADAMS, A E, LAWLOR, M A and ZAKHARIA, M E 'SAMI: a low-frequency prototype for mapping and imaging of the seabed by means of synthetic aperture' *IEEE J of Oceanic Engineering* **24**(1), Jan 1999, 4-15.
8. SHERIFF, R W, 'Synthetic aperture beamforming with automatic phase compensation for high frequency sonars'. *Proc 1992 Symposium on Autonomous Underwater Vehicle Technology, June 1992, 236-245.*
9. PINTO, M A, FOHANNO, F, TREMOIS, O, GUYONIC, S. 'Autofocusing a synthetic aperture sonar using the temporal and spatial coherence of seafloor reverberation', in *High frequency acoustics in shallow water*, ed N G Pace (1997) (*Saclantcen Conf. Proc. CP-45), 417-424.*
10. BELLETTINI, A, and PINTO, M A. 'Theoretical accuracy of synthetic aperture sonar micronavigation using a displaced phase centre antenna' submitted to *IEEE J of Oceanic Engineering,* 2000.
11. PINTO, M., FIORAVANTI, S. and BOVIO, E. 'Accuracy of synthetic aperture sonar micronavigation using a displaced phase centre antenna' SACLANTCEN Report No. SM-352 (undated).
12. BILLON, D and FOHANNO, F. 'Theoretical performance and experimental results for synthetic aperture sonar self-calibration', *Proceedings of Oceans'98 IEEE/OES*, **2**, 965 – 970, 1998, Nice.
13. EICHEL, P H, GHIGLIA, D C, and JAKOWATZ, Jr, C V. 'Speckle processing method for synthetic aperture radar phase correction' *Optics Letters* **14**(1), 1999, 1-3.
14. WAHL, D E, EICHEL, P H, GHIGLIA, D C and JAKOWATZ, Jr, C V. 'Phase gradient autofocus – a robust tool for high-resolution SAR phase correction' *IEEE Trans on Aerospace and Electronic*

Systems, **30**(3), July 1994, 827-835.
15. EICHEL, P H and JAKOWATZ, Jr, C V. 'Phase gradient algorithm as an optimal estimator of the phase derivative' *Optics Letters* **14**(20), 1989, 1101-1103.
16. JAKOWATZ, Jr, C.V., WAHL, D.E., EICHEL, P.H., GHIGLIA, D.C. and THOMPSON, P.A. 'Spotlight-mode synthetic aperture radar: a signal processing approach'. Kluwer academic publishers, 1996.
17. ROBINSON, J. and EMBLEN, C. 'Submarine launched mine reconnaissance system (expanding the MCM role)'. *Proceedings UDT*, Hamburg, May 2001.